https://doi.org/10.30799/jespr.241.24100101 J. Environ. Sci. Pollut. Res. - Volume 10 Issue 1 (2024) 485–491

ISSN: 2455-0272

Share Your Innovations through JACS Directory

Journal of Environmental Science and Pollution Research

Visit Journal at https://www.jacsdirectory.com/jespr

Fabrication and Characterization of Photocatalyst Pb_3CdO_7 for Degradation of Azure-A

Dushyant Kumar Prajapati, Jeevan Kunwar Chouhan, Jinesh Menaria, Tejveer Singh Tanwer, Saroj Lohar, Shipra Bhardwaj*

Department of Chemistry, Government Meera Girls College, Mohanlal Sukhadia University, Udaipur – 313 001, Rajasthan, India.

ARTICLEDETAILS

Article history:
Received 18 April 2024
Accepted 25 April 2024
Available online 03 June 2024

Keywords:
Photocatalysis
Photo-Degradation
Kinetic Study
Scavenger Study

ABSTRACT

Present work comprises of fabrication of the novel Pb_3CdO_7 ternary oxide composite from the corresponding precursors using a co-precipitation approach and calcined. The as-prepared material is then characterized by FTIR, FE-SEM, XPS, EDX, XRD, HR-TEM etc. analytical methods. Based on UV-Vis-NIR spectroscopy, the composite's direct energy band gap is determined to be 5.23 eV, which makes it an effective photocatalyst. The prepared photocatalyst is found to degrade Azure-A dye with an efficiency of up to 94.87%. Scavenger study suggests the participation of active free radicals $O_2^{\bullet-}$ (superoxide anion radical) as the responsible species in breakdown of the dye molecules. The operating parameters are controlled to maximize the photodegradation and a kinetic study is carried out. Used photocatalyst is recycled and is found to work at the same pace for up to five cycles.

GRAPHICAL ABSTRACT

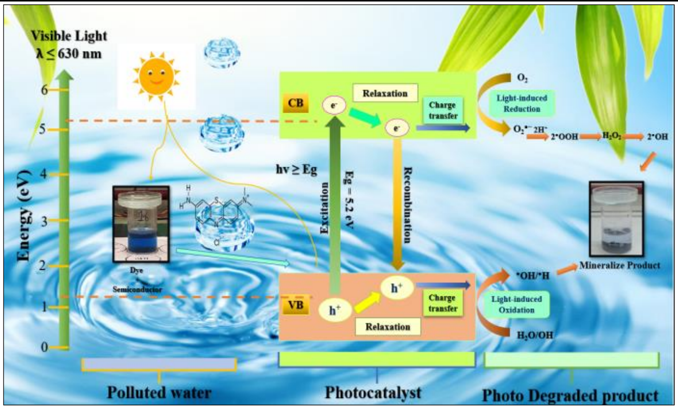

1. Introduction

Water pollution is the major cause in deteriorating the quality of water worldwide, especially in developing countries. Thus, organic pollutant degradation from water, especially potable water becomes necessary. Various methods like filtration, sedimentation, biodegradation etc. were carried to get rid of these pollutants but the success rate was lower. Over decades ago, early observations of titania-based paints chalking and research on metal oxides darkening, when in contact with organic chemicals in sunlight, initiated the study of photocatalysis and developed into one that has conducted a great deal of research over the years. Titania, the photocatalyst that was the subject of most studies, became significant then [1]. An extensive review was conducted on metal oxide nanoparticles and their composites in the context of water remediation [2]. Nakata et al. [3] carried a succinct overview of the state of TiO_2 photocatalysis and discussed structurally regulated TiO_2 photocatalysts that fall into one of four categories: zero, one, two, or three dimensions. Using titanium dioxide as a "model" semiconductor, advancements in the study and use of heterogeneous semiconductor photocatalysis for the treatment of low-level concentrations of contaminants in water and air were carried out [4]. The removal of resistant organic compounds from water through the intimate coupling of the photocatalysis and biodegradation (ICPB) process was carried out by Li et al. [5].

Earlier, metal oxide semiconductors were broadly classified into three groups: zinc oxide, titanium dioxide and other metal oxides, which include cerium oxide, vanadium oxide, tungsten oxide, molybdenum oxide, and indium oxide [6]. Later on, with advancements in studies, a combination of various oxides came into existence and were then classified as binary, ternary, and quaternary photocatalysts. Yao et al. [7] stated that semiconductor-based photocatalysts have drawn the attention of researchers due to their applications in environmental pollution mediation and solar energy conversion. Maddahfar et al. [8] carried out a study of semiconductor and sensor technology in heterogeneous catalysis.

It was surveyed that various sources of water which are near to colouring industries, are much polluted due to excretion of colouring agent especially synthetic dyes in to them. In due course of time, looking to the benefits of these materials towards removal of these dyes, various methods were employed for their synthesis. nanocomposite ZnO-TiO_2 powders of varying ZnO /TiO_2 molar ratios was prepared and used it for decolorization of an azo dye brilliant golden yellow. It was stated that the process follows pseudo-first-order kinetics [9]. Kamaraj et al. [10] prepared a p-type CuO/n-type Pb_2O_3 heterojunction photocatalyst by a simple wet chemical process and the photocatalytic ability was evaluated for the degradation of Rose Bengal (RB) under visible light irradiation. Lead Oxide (PbO) nanoparticles and the composite form of PbO with CdO and ZnO were prepared by the wet chemical method and the crystal structure, optical absorption, and functional groups of the prepared

*Corresponding Author:shiora4ever@gmail.com(Shipra Bhardwaj)

https://doi.org/10.30799/jespr.241.24100101

Cite this Article as: Dushyant Kumar Prajapati, Jeevan Kunwar Chouhan, Jinesh Menaria, Tejveer Singh Tanwer, Saroj Lohar, Shipra Bhardwaj, Fabrication and characterization of photocatalyst Pb_3CdO_7 for degradation of Azure-A, J. Env. Sci. Pollut. Res. 10(1) (2024) 485–491.

materials were also studied [11]. Naeem et al. [12] prepared a SnO_2-Mn_2O_3 binary composite thin-film electrode by a single-step solution-based aerosol-assisted chemical vapour deposition (AACVD) technique.

Elayaraja et al. [13] synthesized cerium (Ce)-doped CdO nanoparticles (NPs) by simple chemical precipitation methods. The photocatalytic degradation efficiency of methyl orange dye at the optimum content of Ce^{3+}-doped CdO-NPs was studied. Murugadoss et al. [14] synthesized quaternary-based zinc-lead-cadmium-copper oxide (ZnO-PbO-CdO-CuO) nanocomposite by a feasible 'one-pot' chemical method. Structural, morphological, and optical properties of nanocomposite was explored using various characterization techniques. They further studied the photocatalytic dye degradation activity by employing two model dyes namely, Fast Green (FG) and Rose Bengal (RB) under sunlight irradiation.

Liu et al. [15] studied Dual Z-scheme $g\text{-}C_3N_4/Ag_3PO_4/Ag_2MoO_4$ ternary composite photocatalyst for solar oxygen evolution. Guo et al. [16] synthesized the novel ternary $AgBr/Ag/PbBiO_2Br$ Z-scheme photocatalyst and it was employed for the degradation of rhodamine B (RhB) and antibiotic bisphenol A (BPA) under visible light irradiation. Chen et al. [17] prepared a Z-scheme $ZnTiO_3/Zn_2Ti_3O_8/ZnO$ ternary photocatalyst by the solvothermal-calcination method and the influence of different reaction temperatures on the crystal phase structure, photoelectrochemical properties, and photocatalytic activities of the samples were investigated. Divya et al. [18] investigated a quaternary $TiO_2/ZnO/RGO/Ag$ nanocomposite that exhibited enhanced photo-activity for the degradation of rhodamine B under visible light. Perovskite-like photocatalyst, $PbBiO_2Br/PbO/g\text{-}C_3N_4$ was synthesized and characterized by Wang et al. [19]. The as prepared material was studied further for its visible-light-driven photocatalytic activity. Synthesis, optical properties and efficient photocatalytic activity of CdO/ZnO hybrid nanocomposite was under taken by Reddy et al. [20]. Flake-like $CuMn_2O_4$ (Copper manganite) Nanoparticles (NPs) were prepared by the Co-precipitation method and the energy band gap was found to be 2.54 eV [21]. The photocatalytic degradation efficiencies were found to be 86% and 92% for methylene blue and malachite green respectively.

Transition metal spinel-type mixed oxides ($FeCo_2O_4$, $MnCo_2O_4$, and $ZnCo_2O_4$) nano-catalysts were synthesized via the co-precipitation route [22]. The photocatalytic potency of synthesized nano-catalysts was examined for an aqueous solution of methylene blue under visible light where as a simple co-precipitation method followed by calcination was adopted to synthesize ZnCdSO ternary semiconductor photocatalyst [23]. The photoactive ternary ZnO–CdS–CdO composite offered a significantly photostable superior photocatalyst property for efficient dye degradation under visible light. The $ZnO/CuO/SnO_2$ nanocomposite was synthesized and characterization was done by various techniques [24]. It was then applied to degrade the fast-green dye under visible light irradiation and exhibited 93.68% degradation efficiency within a short period.

Graphitic carbon nitride ($g\text{-}C_3N_4$) was synthesized and used as photocatalyst by Tai et al. [25] The results showed that the degradation rate of tetracycline was the highest when the material was synthesized at the ratio of 1:1 under the action of a UV lamp and $C_2H_2O_4$, which could reach 99%. Tubular $g\text{-}C_3N_4$ (TCN) with porous structure was prepared by an acid-induced-assembly step. 97.15 % RhB and 62.3 % TC degradation were achieved within 60 minutes. $Bi_2WO_6/ZnIn_2S_4$ was used for the degradation of Rhodamine B (RhB) by Wu et al. [26]. Single-atom Pd on $g\text{-}C_3N_4$ with carbon vacancies towards enhanced photocatalytic NO conversion was carried out by Liu et al. [27]. To improve photocatalytic activity and maximize solar energy use, a new composite material Fe_2O_3/P_2Mo_{18} was prepared by combining polyoxometalates (P_2Mo_{18}) with Fe_2O_3 nanosheets [28].

It was observed that ternary oxides have been working as excellent photocatalyst but are fewer in number and are less used for removal of carcinogens especially dyes from water. Thus, a novel photocatalyst Pb_3CdO_7 was synthesized and examined for structural characteristics, phase purity, surface morphology, etc. by various analytical techniques. The prepared oxide composite was then used for the degradation of various pollutants from water in a heterotic manner and here reporting a systematic kinetic study of removal of carcinogenic dye Azure A which implies as a role model.

2. Experimental Methods

2.1 Characterization

X-ray diffraction (XRD) analysis was carried to ascertain the crystal size of prepared Pb_3CdO_7 (Panalytical X Pert Pro, X-ray diffractometer using Ni-filtered Cu Ka radiation at a scan range of 10\2h\80, at 10 kV and 80 mA for monochromatized Cu Ka (k = 1.5418 Å) radiation). FE-Scanning electron microscopy (FE-SEM) measurements as well as energy dispersive X-ray spectroscopy (EDX) was carried out (Nova Nano FE-SEM 450 (FEI) scanning electron microscope) to investigate the morphology and surface roughness of the sample. XPS spectra was carried for determining the oxidation state of the elements present in the photocatalyst (Physical Electronics Model- PHI 5000 Versa Probe III analysis). Fourier transform infrared (FT-IR) spectra was recorded on an FT-IR Spectrum 2 (Perkin Elmer) spectrophotometer in KBr pellets in the range 400–4000 cm^{-1} to determine the metal oxide bond type. UV–VIS diffuse reflectance spectra was carried on a UV–vis-NIR spectrophotometer (Perkin Elmer, U.S.A.) for calculation of band gap. HRTEM was used for a high-resolution transmission electron microscope and was carried on Tecnai G20 S-TWIN (FEI).

2.2 Materials

All the chemicals were of analytical grade (> 99 %) and were used without further purifications, including lead nitrate hexahydrate (Pb $(NO_3)_2.6H_2O$, Molechem Co., Ltd., 99%), Cadmium nitrate tetrahydrate (Cd $(NO_3)_2{\cdot}4H_2O$, Merck Co., Ltd., 99.5%). Ethanol absolute (CH_3CH_2OH, 99.9%), and sodium hydroxide pellets (NaOH, 96%, Merck Co. Ltd.). Azure-A dye, EDTA, ether, isopropyl alcohol, sulphuric acid, hydrochloric acid, etc. were of CDH make.

2.3 Synthesis of Ternary Pb_3CdO_7 Nanoparticles

A novel photocatalyst Pb_3CdO_7 was prepared by the co-precipitation method, from precursors. 0.1 molar solution of lead nitrate (3.31 g/L, pH 5.2 at 26 °C) and 0.1 molar solution of cadmium nitrate were prepared (3.08 g/L, pH 5.8 at 26 °C). The mixture of the above solutions was then stirred continuously on a magnetic stirrer for 20 minutes. Then a pre-standardized NaOH solution was added drop-wise to the mixture with continuous stirring to obtain the precipitate. The complete precipitate was obtained at pH 10.0. This was then stirred for another 1 h and was allowed to settle. The obtained precipitate was filtered and washed and the supernatant liquid was checked for further precipitation and for the presence of the elements lead and cadmium. The obtained precipitate was exposed to microwave irradiation. The resulting powder was then subjected to the furnace for 5 h at 350 °C for calcination. Off-white crystalline powder of Pb_3CdO_7 was obtained with 88% yield. Fig. 1 shows the flow chart of the process.

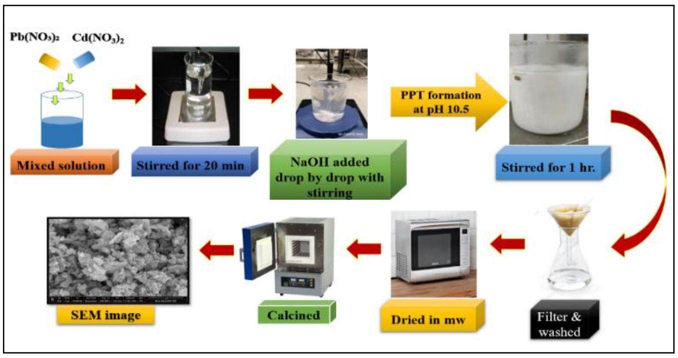

Fig. 1 Flow chart of synthesis of Pb_3CdO_7 photocatalyst

2.4 Photocatalytic Degradation Study

Certain amount of photocatalyst was added to Azure A dye solution at particular pH and was kept under UV-Vis irradiation utilizing a tungsten arc lamp. The absorbance of the dye was monitored using a UV–Vis spectrophotometer (CHINO) by observing the intensity of the absorption band at different time intervals. A typical run i.e. plot between 1+log O.D. (optical density) v/s time. Maximum degradation conditions were extracted by k values at different operational conditions. The percentage of degradation was calculated by,

$$\text{Percent degradation} = (Co - C)/Co \ X\ 100$$

where C_o and C represent the initial concentration and final concentration of the dye at different time intervals, respectively.

3. Results and Discussion

3.1 X-Ray Diffraction Analysis

XRD analysis was carried out and its diffraction spectrum is shown in Fig. 2. The peaks were found at 28° (101), 29° (111), 30.3° (222), 33.08° (202), 38.3° (210), and 56.2° (220) which were found in good correlation with the reported standard XRD peaks of its precursors PbO and CdO [29-

https://doi.org/10.30799/jespr.241.24100101

32]. Peak broadening of diffraction spectra at base indicates the formation of hydroxide within the composites. The strong peaks of each plane dictate well crystalline nature of the prepared material.

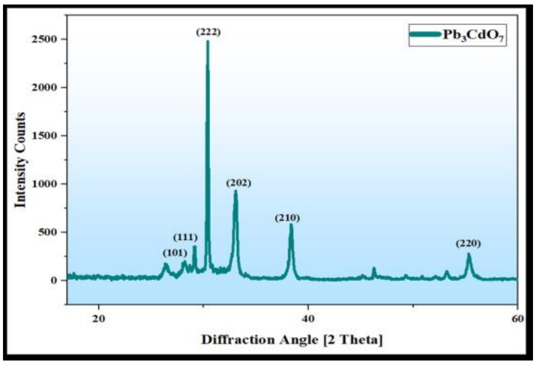

Fig. 2 XRD pattern of Pb_3CdO_7

The average crystal size of the prepared photocatalyst was determined by the XRD (Panalytical X Pert Pro). The data are given in Table 1 and calculated through the Debye-Scherer's formula and the crystallite size of 44.51 nm proved the nano-size and absence of other peaks endorse remarkable crystallinity of the composite material.

Table 1 Crystal size of Pb_3CdO_7

Peak No.	Angle 2θ	FWHM	Crystallite size (nm)	Average crystal size (nm)
1.	29.1354	0.1476	58.11	
2.	30.3975	0.1476	58.27	44.51
3.	33.0848	0.3542	24.45	
4.	38.3870	0.2362	37.21	

3.2 FESEM and EDX Analysis

The SEM analysis of the Pb_3CdO_7 photocatalyst was carried out to investigate the morphology and surface roughness of samples. The images and elemental mapping are given in Fig. 3 which clearly show the presence of elements in homogeneous cluster form and arranged in an organized manner. The grains are present in round shape with some rectangular embedded crystals as well.

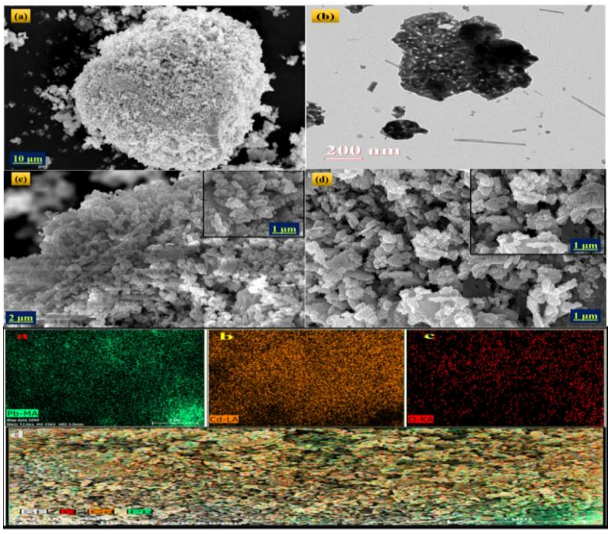

Fig. 3 FESEM images and elemental mapping of Pb_3CdO_7

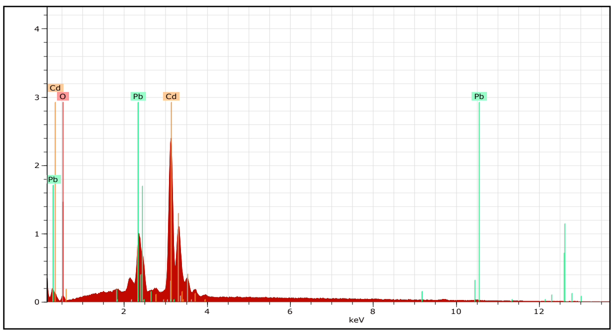

Fig. 4 EDX spectra of Pb_3CdO_7

EDX analysis for composition was carried out and is given in Fig. 4. It reveals the presence of three elements Pb, Cd, and O. The intensity of peaks suggests the ratio to be 3.0:1.0:7.3 for Pb: Cd:O respectively. The values are in good agreement with the proposed formula Pb_3CdO_7.

3.3 XPS Analysis

XPS analysis was carried out to determine the chemical environment of the present elements in the prepared composite. The observations are shown in Fig. 5. The transition peaks involving the Pb 4f, Cd 4f, and O 1s orbitals suggests that the catalyst is composed of Pb, Cd, and O elements. The spectra derived for Pb 4f when de-convoluted showed peaks of binding energies at 137.2 and 142.6 eV, ascribed to Pb (II) 4f 7/2 and 4f 5/2 and could be attributed to Pb existing in a Pb^{2+} oxidation state [33,34]. The binding energy peak of 404.1 and 410.7 eV in next de-convoluted spectra corresponds to that of Cd in the composite and stands for Cd 3d 5/2 and 3d 3/2 transition states suggesting the presence of Cd (II) [32]. The asymmetric peak of the 1s spectra of O was observed at 528.6 [19,20] which can be attributed to the presence of bound oxygen on the surface of nanocrystals due to the formation of PbO-CdO nanocomposite

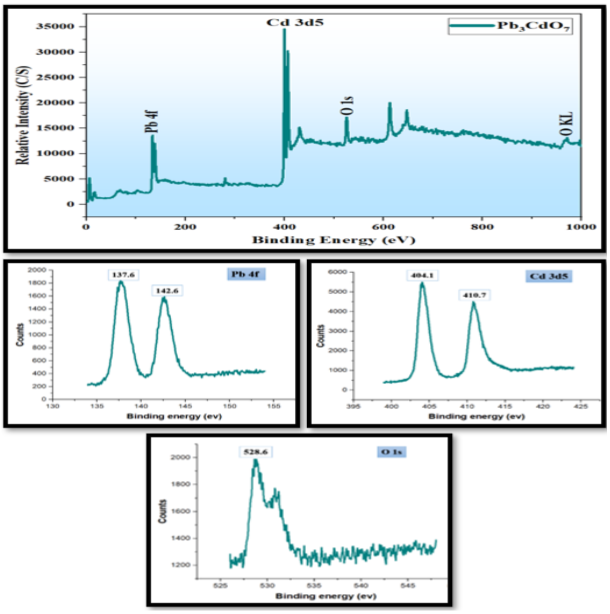

Fig. 5 XPS spectra and convoluted XPS spectra of individual element in Pb_3CdO_7

3.4 FTIR Spectroscopic Analysis

The FTIR spectroscopic analysis was carried out and the study suggests the crystalline and nano powder nature of the prepared photocatalyst. Fig. 6 shows major peaks at 458.57, 532, 684, 1220, 1384.31, 1631.77, 1713.64 and 3441.97 cm^{-1}. The bands in the range of 600–1000 cm^{-1} are generally attributed to the metal–oxygen stretching while in the range of 400–600 cm^{-1} are attributed to M-O bending vibrations. The peaks at 3441.97 cm^{-1} and 1631.77 cm^{-1} are assigned to surface hydroxyl and the band at 1384.31 cm^{-1} is due to OH bending [32,35]. The peak at 532 cm^{-1} indicates the presence of oxides stretching and bending vibrations in PbO, 684 cm^{-1} is attributed to Pb-O vibrations while the characteristic absorption peak observed at 458.57 cm^{-1} is assigned to the stretching band of Pb-O [21,36]. The peak observed at 684 cm^{-1} and a few low-intensity peaks are indications of Cd-O stretching and bending vibrations [35-37]. A general shift in peaks has been observed. All peaks are sharp stating the presence of strong stretching vibrations and denying the presence of impurities.

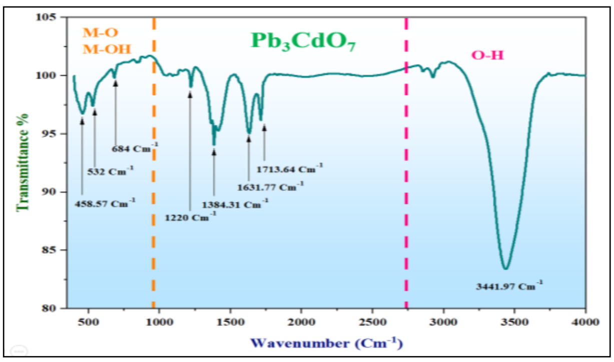

Fig. 6 FTIR spectra of Pb_3CdO_7

https://doi.org/10.30799/jespr.241.24100101

3.5 UV-VIS NIR Spectroscopic Analysis

Electronic transitions occurring within the molecules can be investigated through UV-visible-NIR spectroscopy. The UV-VIS-NIR spectrum of the synthesized photocatalyst Pb_3CdO_7 was investigated in the 200 to 800 nm UV-visible-NIR range and the spectrum is given in Fig. 7. Broad absorption bands found at 187.3 nm and 232.97 to 255.22 nm, represent the peaks for PbO and CdO respectively.

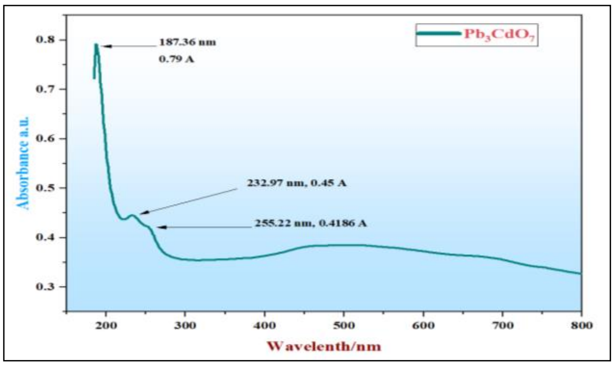

Fig. 7 UV-VIS-NIR spectra of Pb_3CdO_7

Band gap energy of a material is strongly dependent on the dimensions, size, and shape of the material. Precisely estimating the band gap energy is essential for forecasting the photo-physical and photochemical characteristics of a semiconductor as is its capability to excite and generate electron and hole pairs for a redox reaction to proceed. Fig. 8 shows use of UV-Vis-NIR spectra for calculation of band gap value. It is obtained by extrapolating the linear part at $(h\nu)^2 = 0$ from Plot $(\alpha h\nu)^2$ v/s $h\nu$ and is found to be 5.23 eV.

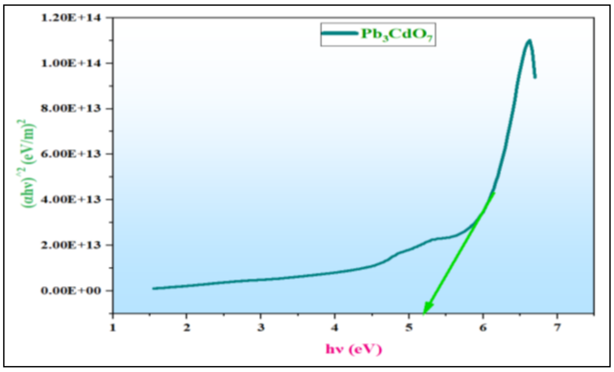

Fig. 8 TAUC plot for Pb_3CdO_7

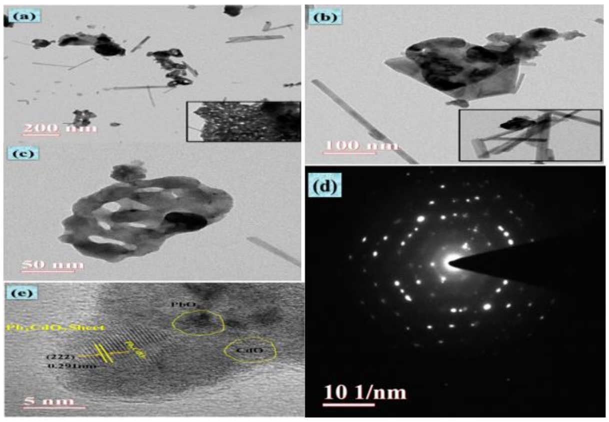

Fig. 9 HR-TEM images of Pb_3CdO_7

3.6 HR-TEM Analysis

High-resolution transmission electron microscopy (HR-TEM) images were used to study the morphology of Pb_3CdO_7 nanocomposite and to gain a better understanding of the structural characteristics of the nanoparticles. The selected-area electron diffraction (SAED) pattern of the Pb_3CdO_7 nanocomposite is shown in Fig. 9. The diameters of crystallites measured by HR-TEM and those determined by powder XRD analysis appeared in good correlation. HR-TEM pictures show the needle as well as rectangular shape of the prepared nanoparticles. The particle sizes of the material varied from 50 nm to 200 nm. Somewhere a two-dimensional sheet structure is also observed. A black patch on each hexagonal ring face shows formation of PbO core. The formation of a transparent layer on the black core surface is sign of CdO coating [37]. Furthermore, a ring pattern free of any additional diffraction spots is showcased, which is a characteristic of the crystallites that comprise the structure of the nanocomposite. The present synthesis approach is found effective in producing nanoparticles with a consistent particle size distribution.

3.7 Kinetic Study of Photocatalytic Degradation of Azure-A Dye

The photocatalytic performance of Pb_3CdO_7 was examined under solar light irradiation by degrading Azure-A dye. 0.18 g of the photocatalyst was added to 50 mL of 0.4×10^{-4} M solution of Azure-A in a beaker, pH of the solution was adjusted at 10.5 and was kept under UV-Vis irradiation utilizing a 250 W tungsten arc lamp. A water cut off filter was used to avoid heat reaction. The photocatalytic degradation study was investigated by spectrophotometer at 630 nm (λ_{max}). Fig. 10A depicts a plot of percentage degradation v/s time where after 55 minutes of exposure to light, in the presence of Pb_3CdO_7, degradation reached up to 94.87%. Fig. 10B shows the error bar for the typical run. Langmuir-Hinshelwood model was used for the kinetic study of the reaction and is described as:

$$r = -dC/dt = kKc/(1 + KC)$$

where r is the rate of reaction (mol/Lmin), C is the equilibrium concentration of the reagent (mol/L), t is the time (min), k is the rate constant (L/min), and K is the Langmuir constant (L/mol). It is simplified further to the following pseudo-first-order expression:

$$\ln(C_o/C_t) = kt$$

where C_t and C_o are dye concentrations at time t and t = 0, respectively, k is the pseudo-first-order rate constant (min^{-1}).

The results revealed excellent linear correlation, implying that the reaction follows pseudo-first order. The rate constant for the degradation reaction was determined as 4.51×10^{-4} sec^{-1} at maximum degradation conditions that are pH = 10.5, [Azure A] = 0.4×10^{-4} M, amount of semiconductor = 0.18 g and light intensity = 1530 mW/cm^2.

Various factors affecting the rate of reaction were studied to extract the maximum degradation conditions by varying their measures that are discussed hereby.

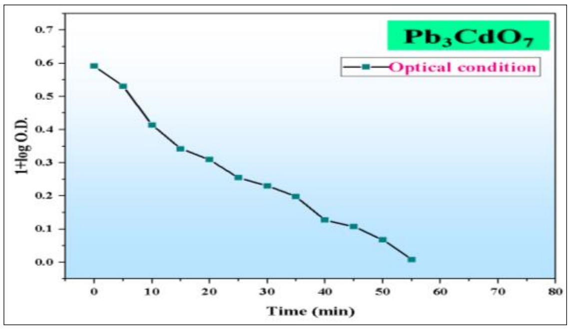

Fig. 10A Typical run for photocatalytic degradation of Azure A by Pb_3CdO_7 photocatalyst

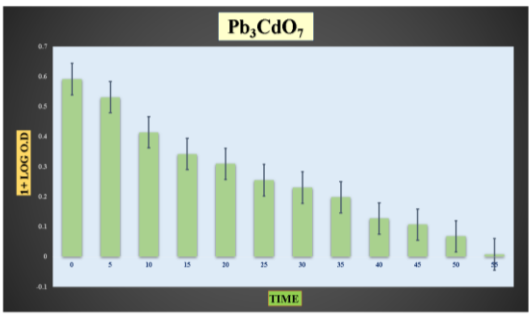

Fig. 10B Error bar graph for typical run

3.7.1 Effect of pH

Effect of pH on dye degradation was examined at various pH values ranging from 5 to 11 keeping all other variables constant. The outcomes are reported in Fig. 11 and values of rate constant (k) are given in Table 2. Dyes are pH sensitive and it is well depicted in the figure by change in optical absorbance. According to the findings, after 55 minutes of visible irradiation, the photocatalytic degradation efficiency was 94% at pH 10.5. The increase in the rate of degradation is observed due to the formation of

https://doi.org/10.30799/jespr.241.24100101

greater number of $O_2^{-\bullet}$ free radicals which initiates and carries forward the photocatalytic degradation reaction and is expressed in the mechanism. With further increase in pH, the solution becomes opaque, working as an obstacle in the path of incident light reaching the surface of the photocatalyst, thus a decrease in the rate is observed

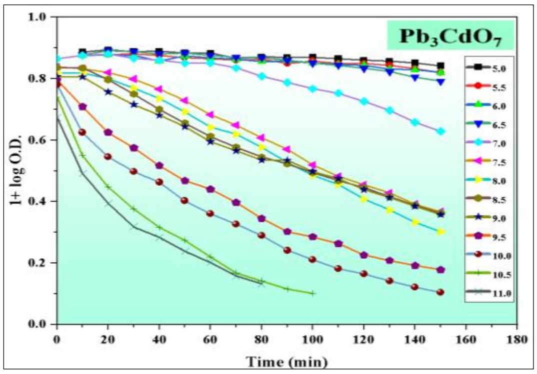

Fig. 11 Effect of pH on dye degradation

Table 2 Rate constant at different pH values

S.No.	pH	Rate Constant k × 10^{-4} (sec^{-1})
1.	5.0	0.0063
2.	5.5	0.0064
3.	6.0	0.0095
4.	6.5	0.0168
5.	7.0	0.77
6.	7.5	1.77
7.	8.0	1.90
8.	8.5	2.46
9.	9.0	2.35
10.	9.5	2.91
11.	10.0	3.09
12.	10.5	4.51
13.	11.0	3.93

3.7.2 Effect of Dye Concentration

The effect of dye concentration was studied by varying it from 0.4 to 1.8 x 10^{-4} M while all other factors were kept constant. The results are summarized in Fig. 12 and rate constants (k) are mentioned in Table 3. The photocatalytic degradation efficiency was 90, 63, 64, 68, 79, 76, 75, and 52% at 0.4, 0.6, 0.8, 1.0, 1.2, 1.4, 1.6 and 1.8 x 10^{-4} M dye concentrations respectively. This indicates an inverse relationship between the dye concentration and the photocatalytic degradation efficiency. This is because as the dye concentration increases, it imparts a darker color to the solution that stops the desired solar radiations reaching the photocatalyst surface, thus the production of O_2^{-} free radicals is hindered causing rate reduction.

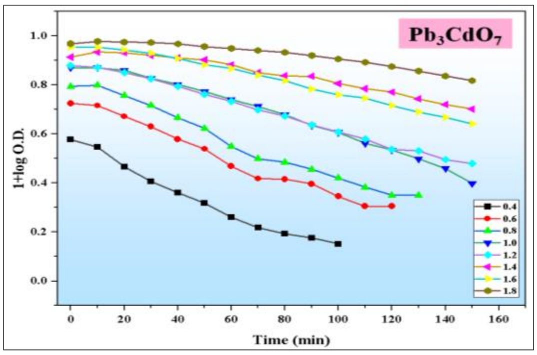

Fig. 12 Effect of dye concentration (mol/L)

Table 3 Rate constant at different dye concentrations

S.No.	Concentration × 10^{-4} (M)	k × 10^{-4} (sec^{-1})
1.	0.4	4.51
2.	0.6	3.74
3.	0.8	2.54
4.	1.0	2.13
5.	1.2	2.25
6.	1.4	1.45
7.	1.6	1.66
8.	1.8	0.66

3.7.3 Effect of Photocatalyst Loading

The effect of photocatalyst dose ranging from 0.8 to 3.6 g/L, was evaluated and all other factors were kept constant. The findings are given in Fig. 13 and rate constants (k) are tabulated in Table 4. The results showed that the degradation efficiency obtained was 76,78,78,70,74,79,81 and 84% for the applied catalyst dosages of 0.8, 1.2, 1.6, 2.0, 2.4, 2.8, 3.2 and 3.6 g/L respectively. This direct relationship between the catalyst dose and the effectiveness of photocatalytic degradation is most likely attributable to more surface area of the photocatalyst available for irradiation and an increase in the generation of the O_2^{-} free radical is observed. Thus, an increased rate of reaction is attained. Further addition of the photocatalyst did not increase the rate and degradation, rather added a layer to the surface of photocatalyst.

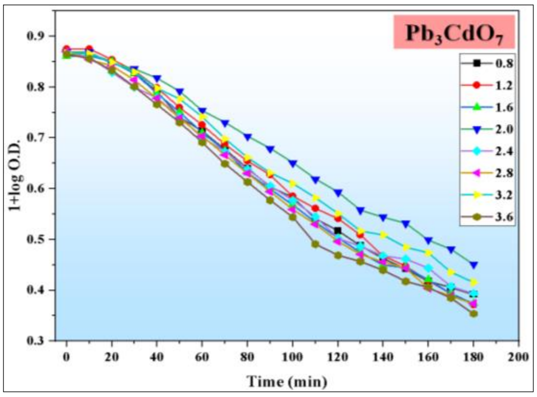

Fig. 13 Effect of photocatalyst doses (g/L)

Table 4 Rate constant at different amount of photocatalyst

S.No.	Amount of photocatalyst (g/L)	k × 10^{-4} (sec^{-1})
1.	0.04	4.09
2.	0.06	3.95
3.	0.08	4.33
4.	0.1	2.99
5.	0.12	4.26
6.	0.14	4.13
7.	0.16	3.17
8.	0.18	4.51

3.7.4 Effect of Intensity of Light

With all other factors remaining constant, the effect of variation of the light intensity on dye degradation was studied. The data are represented in Fig. 14 and rate constant (k) values are shown in Table 5. Above 1530 mW/cm², it was observed that heat reaction starts dominating so further study with increased intensity was avoided. Fig. 14 states that the degradation of pollutants increases with an increase in light intensity. Since electron-hole production dominates and electron-hole recombination reduces at higher intensities, the rise in degradation was noticeably higher.

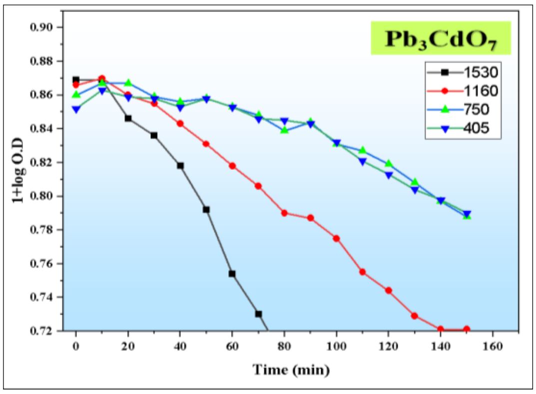

Fig. 14 Effect of intensity of light (mW/cm²)

Table 5 Rate constants at different light intensities

S.No.	Light Intensity (mW/cm²)	k × 10^{-4} (sec^{-1})
1.	1530	4.51
2.	1160	1.76
3.	750	0.57
4.	405	0.41

https://doi.org/10.30799/jespr.241.24100101

Cite this Article as: Dushyant Kumar Prajapati, Jeevan Kunwar Chouhan, Jinesh Menaria, Tejveer Singh Tanwer, Saroj Lohar, Shipra Bhardwaj, Fabrication and characterization of photocatalyst Pb_3CdO_7 for degradation of Azure-A, J. Env. Sci. Pollut. Res. 10(1) (2024) 485–491.

3.7.5 Effect of Scavenger on Dye Degradation

A scavenger test was carried out to determine the active species participating in the degradation process. A 3% solution of EDTA (superoxide anion radical scavenger) was added to the reaction mixture and was then exposed to light. It was observed that this ceases the reaction almost completely with a slight degradation of 2.74%. The carried comparative study with different scavengers and % degradation is shown in Fig. 15. It demonstrates that OH free radicals and $O_2^{\bullet-}$ super oxide anion free radicals are produced during the course of the reaction and are responsible species the photocatalytic degradation of the dye.

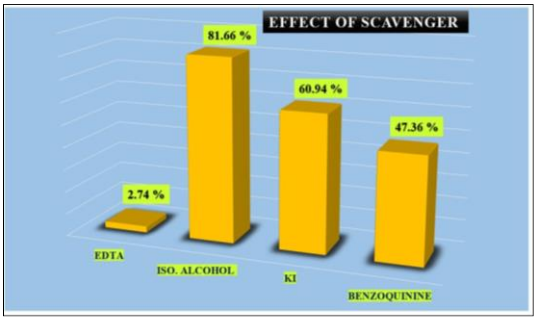

Fig. 15 Scavenger study

3.7.6 Recycle Experiment

The efficiency of Pb_3CdO_7 nanoparticles was checked by repeating the degradation experiment after calcining the used material under identical conditions. The photocatalyst did not show any overt signs of wear and tear after four cycles. The rate constant of Pb_3CdO_7 composite was determined as 4.12×10^{-4} sec^{-1}, 3.88×10^{-4} sec^{-1}, 3.66×10^{-4} sec^{-1}, 3.66×10^{-4} sec^{-1} after first, second, third and fourth recycle respectively at maximum degradation conditions.

3.7.7 Mechanism Proposed

After carrying out all the experiments and obtaining concrete results, a mechanism of degradation is proposed, based on outcomes that the scavenger test ascertained the participation of active oxidizing species super oxide anion free radical and the lab test used to ascertain the end product which stated complete degradation of dye into smaller fragments like CO_2, H_2O, NO_2, N_2, etc. This concluded in the mechanism as:

$$Pb_3CdO_7 + h\nu\ (\text{photon}) \rightarrow Pb_3CdO_7\ (e^- + h^+) \quad (6)$$
$$h^+ + OH^- \rightarrow OH^\bullet \quad (7)$$
$$e^- + O_2 \rightarrow O_2^{\bullet-} \quad (8)$$
$$H_2O + O_2^{\bullet-} \rightarrow HOO^\bullet + OH^\bullet \quad (9)$$
$$2OOH^\bullet \rightarrow O_2 + H_2O_2 \quad (10)$$
$$H_2O_2 + O_2^{\bullet-} \rightarrow OH^\bullet + OH^- + O_2 \quad (11)$$
$$OH^\bullet + h\nu + \text{pollutant} \rightarrow \text{degraded product} \rightarrow CO_2 + N_2 + NO_2 + H_2O \ldots (12)$$

Formation of $O_2^{\bullet-}$ is endorsed in number of studies [38-40]. Scientists stated that photogenerated electrons were absorbed by oxygen on the surface of the catalyst to form superoxide radicals. These superoxide radicals again formed two $HOO^\bullet$ radicals, which produced $OH\bullet$ radicals in subsequent steps which plays a key role in the degradation of the dye molecule.

4. Conclusion

It is concluded here by that synthesis of novel Pb_3CdO_7 nanocomposite is carried by a simple co-precipitation method. Various analyses are then employed to determine its properties. The energy band gap for the as-prepared material is ascertained to be 5.2 eV which adds excellent photocatalytic property to it, of not allowing easy recombination of generated electron hole pairs on its surface. The prepared material is further used to trap solar light for degradation of dyes into smaller and harmless fragments. A systematic kinetic study is carried out to obtain maximum degradation condition within time range and it stated that the reaction follows pseudo first order kinetics rule. Scavenger study suggested the participation super oxide free radicals in the reaction and on this basis, mechanism is proposed. Recycling experiment showed that the same material can be used again and again to clean water up to considerable extent. Thus, an excellent route for removal of coloured pollutants from water is incorporated which makes water available for universal use.

References

[1] A. Fujishima, X. Zhang, D.A. Tryk, TiO_2 photocatalysis and related surface phenomena, Surf. Sci. Rep. 63(12) (2008) 515-582.

[2] R. Gusain, K. Gupta, P. Joshi, O.P. Khatri, Adsorptive removal and photocatalytic degradation of organic pollutants using metal oxides and their composites: A comprehensive review, Adv. Colloid Interf. Sci. 272 (2019) 102009.

[3] K. Nakata, A. Fujishima, TiO_2 photocatalysis: Design and applications, J. Photochem. Photobiol. C: Photochem. Rev. 13(3) (2012) 169-189.

[4] A.O. Ibhadon, P. Fitzpatrick, Heterogeneous photocatalysis: recent advances and applications, Catalysis 3(1) (2013) 189-218.

[5] G. Li, S. Park, B.E. Rittmann Developing an efficient TiO_2-coated biofilm carrier for intimate coupling of photocatalysis and biodegradation, Water Res. 46(19) (2012) 6489-6496.

[6] S.H.S. Chan, T. Yeong Wu, J.C. Juan, C.Y. Teh, Recent developments of metal oxide semiconductors as photocatalysts in advanced oxidation processes (AOPs) for the treatment of dye wastewater, J. Chem. Tech. Biotech. 86(9) (2011) 1130-1158.

[7] W. Yao, B. Zhang, C. Huang, C. Ma, X. Song, Q. Xu, Synthesis and characterization of high efficiency and stable Ag_3PO_4/TiO_2 visible light photocatalyst for the degradation of methylene blue and rhodamine B solutions, J. Mater. Chem. 22(9) (2012) 4050-4055.

[8] M. Maddahfar, M. Ramezani, M. Sadeghi, A. Sobhani-Nasab, $NiAl_2O_4$ nanoparticles: synthesis and characterization through modify sol–gel method and its photocatalyst application, J. Mater. Sci. Mater. Electron 26(10) (2015) 7745-7750.

[9] M.A. Habib, M.T. Shahadat, N.M. Bahadur, I.M. Ismail, A.J. Mahmood, Synthesis and characterization of ZnO-TiO_2 nanocomposites and their application as photocatalysts, Int. Nano. Lett. 3(1) (2013) 1-8.

[10] E. Kamaraj, S. Somasundaram, K. Balasubramani, M.P. Eswaran, R. Muthuramalingam, S. Park, Facile fabrication of CuO-Pb_2O_3 nano photocatalyst for efficient degradation of Rose Bengal dye under visible light irradiation, App. Surf. Sci. 433 (2018) 206-212.

[11] H. Sivaram, D. Selva, A. Alsalme, A. Alswieleh, R. Jayavel, Enhanced performance of PbO nanoparticles and PbO-CdO and PbO-ZnO nanocomposites for supercapacitor application, J. Alloys Compd. 731 (2018) 55-63.

[12] R. Naeem, M.A. Mansoor, K. Munawar, A. Adnan, T. Zaharinie, M.N. Mohd Zubir, Versatile Fabrication of Binary Composite SnO_2-Mn_2O_3 Thin Films by AACVD for Synergistic Photocatalytic Effect, J. Elect. Mat. 50(7) (2021) 3897-3906.

[13] M. Elayaraja, I.K. Punithavathy, M. Jothibas, A. Muthuvel, S.J. Jeyakumar, Effect of rare-earth metal ion Ce^{3+} on the structural, optical and photocatalytic properties of CdO nanoparticles, Nanotech. Environ. Eng. 5(3) (2020) 1-10.

[14] G. Murugadoss, K. Thiruppathi, N. Venkatesh, S. Hazra, A. Mohankumar, et al., Construction of novel quaternary nanocomposite and its synergistic effect towards superior photocatalytic and antibacterial application, J. Environ. Chem. Eng. 10(1) (2020) 106961.

[15] W. Liu, J. Shen, X. Yang, Q. Liu, H. Tang, Dual Z-scheme g-C_3N_4/Ag_3PO_4/Ag_2MoO_4 ternary composite photocatalyst for solar oxygen evolution from water splitting, App. Surf. Sci. 456 (2018) 369-378.

[16] H. Guo, C.G. Niu, X.J. Wen, L. Zhang, C. Liang, X.G. Zhang, G.M. Zeng, Construction of highly efficient and stable ternary AgBr/Ag/$PbBiO_2Br$ Z-scheme photocatalyst under visible light irradiation: performance and mechanism insight, J. Colloid Interf. Sci. 513 (2018) 852-865.

[17] F. Chen, C. Yu, L. Wei, Q. Fan, F. Ma, et al., Fabrication and characterization of $ZnTiO_3$/$Zn_2Ti_3O_8$/ZnO ternary photocatalyst for synergetic removal of aqueous organic pollutants and Cr (VI) ions, Sci. Total Environ. 706 (2020) 136026.

[18] K.S. Divya, M.M. Xavier, P.V. Vandana, V.N. Reethu, S. Mathew, A quaternary TiO_2/ZnO/RGO/Ag nanocomposite with enhanced visible light photocatalytic performance, New J. Chem. 41(14) (2017) 6445-6454.

[19] Y.C. Wang, A.H. Lee, C.C. Chen, Perovskite-like photocatalyst, $PbBiO_2Br$/PbO/g-C_3N_4: Synthesis, characterization, and visible-light-driven photocatalytic activity, J. Taiwan Inst. Chem. Eng. 93 (2018) 315-328.

[20] C.V. Reddy, B. Babu, J. Shim, Synthesis, optical properties and efficient photocatalytic activity of CdO/ZnO hybrid nanocomposite, J. Phy. Chem. Solids 112 (2018) 20-28.

[21] L. Nejati-Moghadam, S. Gholamrezaei, M. Salavati-Niasari, A. Esmaeili-Bafghi-Karimabad, Hydrothermal synthesis, and characterization of lead oxide nanocrystal in presence of tetradentate Schiff-base and degradation investigation of organic pollutant in the wastewater, J. Mater. Sci.: Mater. Electron. 28(13) (2017) 9919-9926.

[22] Z. Zhong, Q. Zhang, Y. Zhu, B. Chen, S. Xu, T. Shen, S. Luo, Research progress of Co-based spinel oxide materials for direct methanol fuel cells, New J. Chem. 48 (2024) 7148-7167.

[23] D. Das, P. Nandi, Ternary ZnCdSO composite photocatalyst for efficient dye degradation under visible light retaining Z-scheme of migration pathways for the photogenerated charge carriers. Sol. Energy Mater. 217 (2020) 110674.

[24] A.H. Bhat, H.T. N. Chisti, Facile fabrication of ternary metal oxide ZnO/CuO/SnO_2 nanocomposite for excellent photocatalytic degradation of fast green dye, Int, J. Environ. Anal. Chem. 103(20) (2023) 9594-9615.

[25] G. Tai, G. Li, Z. Cai, Y. Pan, J. Han, J. Shi, G. Wu, Enhanced performance and recyclability for peroxymonosulfate activation via controlling the different morphologies of g-C_3N_4, Colloids and Surf. A: Physicochem. Eng. Asp. 674 (2023) 131925.

[26] G. Wu, Q. Liu, J. Wang, S. Xia, X. Huang, J. Han, W. Xing, Construction of hierarchical Bi_2WO_6/$ZnIn_2S_4$ heterojunction for boosting photocatalytic performance in the degradation of organic compounds and reduction of hexavalent chromium, Colloids Surf. A 653 (2022) 130048.

[27] G. Liu, Y. Huang, H. Lv, H. Wang, Y. Zeng, M. Yuan, C. Wang, Confining single-atom Pd on g-C_3N_4 with carbon vacancies towards enhanced photocatalytic NO conversion, App. Catal. B: Env. 284 (2021) 119683.

https://doi.org/10.30799/jespr.241.24100101

Cite this Article as: Dushyant Kumar Prajapati, Jeevan Kunwar Chouhan, Jinesh Menaria, Tejveer Singh Tanwer, Saroj Lohar, Shipra Bhardwaj, Fabrication and characterization of photocatalyst Pb_3CdO_7 for degradation of Azure-A, J. Env. Sci. Pollut. Res. 10(1) (2024) 485–491.

[28] Y. Zhang, M. Zhao, J. Huang, N. Zhao, H. Yu, Controllable synthesis, photocatalytic property, and mechanism of a novel POM-based direct Z-scheme nano heterojunction α- Fe_2O_3/P_2Mo_{18}, Molecules 28(18) (2023) 6671.
[29] A.V. Borhade, D.R. Tope, B.K. Uphade, An efficient photocatalytic degradation of methyl blue dye by using synthesized PbO nanoparticles, E. J. Chem. 9(2) (2012) 705-715.
[30] A.M. Mebed, A.M. Abd-Elnaiem, A.H. Alshammari, T.A. Taha, M. Rashad, D. Hamad, Controlling the structural properties and optical bandgap of PbO–Al_2O_3 nanocomposites for enhanced photodegradation of methylene blue, Catalysis 12(2) (2022) 142.
[31] M. Batool, R. Gill, K. Munawar, V. McKee, M. Mazhar, Single source precursor derived ZnO–PbO composite thin films for enhanced photocatalytic activity, J. Solid State Chem. 305 (2022) 122642.
[32] P.S. Kumar, M. Selvakumar, P. Bhagabati, B. Bharathi, S. Karuthapandian, S. Balakumar, CdO/ZnO nanohybrids: facile synthesis and morphologically enhanced photocatalytic performance, RSC Adv. 4(62) (2014) 32977-32986.
[33] F.Y. Liu, Y.M. Dai, F.H. Chen, C.C. Chen, Lead bismuth oxybromide/grapheneoxide: synthesis, characterization, and photocatalytic activity for removal of carbon dioxide, crystal violet dye, and 2-hydroxybenzoic acid, J. Colloid Interf. Sci. 562 (2020) 112-124.
[34] A.H. Lee, Y.C. Wang, C.C. Chen, Composite photocatalyst, tetragonal lead bismuth oxyiodide/bismuth oxyiodide/graphitic carbon nitride: synthesis, characterization, and photocatalytic activity, J. Colloid Interf. Sci. 33 (2019) 319-332.
[35] A.M. Abu-Dief, A.A. Essawy, A.K. Diab, W.S. Mohamed, Facile synthesis and characterization of novel Gd_2O_3–CdO binary mixed oxide nanocomposites of highly photocatalytic activity for wastewater remediation under solar illumination, J. Phy. Chem. Solids 148 (2021) 109666.
[36] S. Asha, C. Henry, M.R. Bindhu, A.M. Al-Mohaimeed, M.R. AbdelGawwad, M.S. Elshikh, Improved photocatalytic activity for degradation of textile dyeing wastewater and thiazine dyes using $PbWO_4$ nanoparticles synthesized by co-precipitation method, Environ. Res. 200 (2021) 111721.
[37] V.D. Araújo, R.L. Tranquilin, F.V.D. Motta, C.A. Paskocimas, M.I.B. Bernardi, et al., Effect of polyvinyl alcohol on the shape, photoluminescence and photocatalytic properties of $PbMoO_4$ microcrystals, Mater. Sci. Semicond. Process. 26 (2014) 425-430.
[38] F. Wu, C. Zhou, G. Tai, Y. Ma, X. Yang, Y. Pan, G. Wu, ZIF-67/BiOCl Z-Scheme Heterojunction photocatalyst for photodegradation of organic dyes and antibiotics, ACS App. Nano Mater. 6(19) (2023) 17814-17825.
[39] R. Adhikari, S. Malla, G. Gyawali, T. Sekino, S.W. Lee, Synthesis, characterization, and evaluation of the photocatalytic performance of Ag-$CdMoO_4$ solar light-driven plasmonic photocatalyst, Mater. Res. Bull. 48(9) (2023) 3367-3373.
[40] K. Parida, L. Mohapatra, N. Baliarsingh, Effect of Co^{2+} substitution in the framework of carbonate intercalated Cu/Cr LDH on structural, electronic, optical, and photocatalytic properties. J. Phy. Chem. C 116(42) (2016) 22417-22424.

https://doi.org/10.30799/jespr.241.24100101

Cite this Article as: Dushyant Kumar Prajapati, Jeevan Kunwar Chouhan, Jinesh Menaria, Tejveer Singh Tanwer, Saroj Lohar, Shipra Bhardwaj, Fabrication and characterization of photocatalyst Pb_3CdO_7 for degradation of Azure-A, J. Env. Sci. Pollut. Res. 10(1) (2024) 485–491.